Origin of magnetocrystalline anisotropy oscillations in (001) face-centred-cubic Co thin films and effect of sp–d hybridization

2003 J. Phys.: Condens. Matter 15 29

(http://iopscience.iop.org/0953-8984/15/2/304)

INSTITUTE OF PHYSICS PUBLISHING JOURNAL OF PHYSICS: CONDENSED MATTER

J. Phys.: Condens. Matter **15** (2003) 29–46 PII: S0953-8984(03)53111-3

Origin of magnetocrystalline anisotropy oscillations in (001) face-centred-cubic Co thin films and effect of sp–d hybridization

M Cinal

Department of Mathematics, Imperial College of Science, Technology and Medicine, 180 Queen's Gate, London SW7 2BZ, UK
and
Institute of Physical Chemistry of the Polish Academy of Sciences, ul. Kasprzaka 44/52, 01-224 Warszawa, Poland[1]

E-mail: mcinal@ichf.edu.pl

Received 6 September 2002
Published 20 December 2002
Online at stacks.iop.org/JPhysCM/15/29

Abstract

Magnetocrystalline anisotropy (MA) energy of (001) face-centred-cubic Co(N) films is calculated for film thicknesses $N = 1$–28 in a realistic tight-binding model with and without sp–d orbital hybridization included. The obtained results show that the average MA energy is *not* largely influenced by the sp–d hybridization. On the other hand, the oscillation pattern is remarkably changed when the sp–d hybridization is included: in this case the MA energy has oscillations with a clear period of 2 atomic layers (AL), similar to the previous *ab initio* calculations (Szunyogh L, Újfalussy B, Blaas C, Pustugova U, Sommers C and Weinberger P 1997 *Phys. Rev.* B **56** 14036). A careful analysis in $\boldsymbol{k}$- and N-spaces reveals that the total MA oscillations are a superposition of two oscillatory contributions: one coming from the neighbourhood of the $\overline{\Gamma}$-point with period close to 2 AL (regardless whether the sp–d hybridization is present or not) and the other originating in the region around the $\overline{\mathrm{M}}$-point. The $\overline{\mathrm{M}}$-point contribution has a larger period and its amplitude is significantly smaller than that of the $\overline{\Gamma}$-point contribution when the sp–d hybridization is included so that the 2 AL $\overline{\Gamma}$-point contribution is dominant in this case. The two oscillatory MA contributions are attributed to quantum-well states and the corresponding oscillation periods are related to the extremal radii of the minority-spin bulk Co Fermi surface.

1. Introduction

One of the crucial properties of thin magnetic films is the dependence of energy on the magnetization direction, known as magnetic anisotropy. This dependence arises due to two

[1] Permanent address.

different factors. The first one is *classical* magnetostatic, dipole–dipole, interaction leading to shape anisotropy. The other one is *quantum-relativistic* spin–orbit (SO) coupling through which the energy of an electron depends on the direction of its spin with respect to the film's geometric structure. The later effect is referred to as magnetocrystalline anisotropy (MA). While the energy of shape anisotropy grows linearly with the film thickness the MA energy of films with cubic lattices has been found to be nearly thickness-independent in most experiments (e.g. [1–3]) apart for the possible occurrence of a peak in the MA dependence in the very early stage of film growth [2]. However, only a few experimental papers [4–6] report some MA oscillations. On the other hand, the pronounced oscillations of the MA energy are usually found in theoretical calculations [7–19]. The disagreement between theory and experiment can be attributed to surface roughness and/or interdiffusion present in experimental layered systems. This conjecture still waits to be verified and a theoretical study is under way [20].

The oscillations of MA energy in (001) face-centred-cubic (fcc) Co(N) unsupported slabs and Pd(p)/Co(N)/Pd(p) systems have been found theoretically with a parametrical tight-binding (TB) model by Cinal *et al* [9–13]. Similar MA oscillations in Co/Cu films versus thicknesses of Co and Cu layers have also been obtained within an *ab initio* approach by Szunyogh *et al* [16]. The latter authors analysed the MA oscillations by using the discrete Fourier transformation and thus determined the corresponding oscillation periods with good accuracy. They attributed MA oscillations to Ruderman–Kittel–Kasuya–Yosida (RKKY)-like interactions. On the other hand, it has been proved in [12, 13] that the oscillations of the MA energy versus the Pd overlayer thickness in Co/Pd systems are due to quantum-well (QW) states which exist in the Pd overlayer and cross the Fermi level in the centre of the surface Brillouin zone (BZ). The aim of the present paper is to establish the origin of the MA oscillations in a (001) fcc Co(N) film and, in particular, to examine whether QW states play a similar role in this purely ferromagnetic, system. To this end, the MA energy of (001) fcc Co(N) films is broken down in $\boldsymbol{k}$-space and later analysed as a function of thickness N. In effect, the individual quantum states responsible for the MA oscillations are identified and the corresponding oscillation periods are explained. This method is similar to the one applied previously for the Co/Pd system [13] but it has had to be significantly modified for use in the present study of MA oscillations versus the thickness of the *ferromagnetic* Co film.

The *ab initio* calculations done for (001) fcc systems including the Co(N) layer by Szunyogh *et al* [16] yielded MA oscillations versus the Co layer thickness N with a clear period of 2 atomic layers (AL). On the other hand, the TB, presumably less accurate, model of [9, 11] led to a more complex oscillation pattern. This situation poses a question of why this discrepancy takes place and whether it is possible to obtain the correct, *ab initio*-like, MA oscillations within a TB approach. The present paper shows that it is just neglecting orbitals other than d, as assumed in the previously applied TB model [9, 11], that leads to the incorrect MA thickness dependence for Co films. The calculations reported here are done in two TB models: one includes all nine s, p, d orbitals; the other uses only five d orbitals, but its parameters are derived from the first, nine-orbital, model. The MA results of the two TB models are compared at different stages in order to understand why neglecting s and p orbitals affects the MA oscillations. This problem is especially interesting in view of the usually accepted assumption that magnetic properties of transition metals are attributed to d orbitals.

2. Theory

The investigated system is a (001) fcc Co film which consists of N AL. All layer magnetic moments $\boldsymbol{M}_l$ (per atom) are assumed to be collinear and pointing in a direction characterized by the polar angle θ made with the slab surface normal (the z axis) and by the azimuthal angle

ϕ around the normal. ϕ is measured from the (110) axis which is chosen to be the x axis; the y axis is along the $(\overline{1}10)$ direction. Thus, the x and y directions are along the axes of the square lattice formed by atoms on the (001) fcc surface. The square lattice constant is $a_{2d} = a/\sqrt{2}$, where a denotes the bulk Co fcc lattice constant.

The film electronic structure is described with the extended TB Hamiltonian

$$H = H(\theta, \phi) = H_0 + H_{SO}(\theta, \phi) \tag{1}$$

which, apart from the standard TB Hamiltonian

$$H_0 = \sum_{lj} \sum_{\mu} \sum_{\sigma} V^{\sigma}_{lj\mu} c^{\dagger}_{lj\mu\sigma} c_{lj\mu\sigma} + \sum_{lj} \sum_{l'j'}{}' \sum_{\mu\nu} \sum_{\sigma} T^{\sigma}_{lj\mu,l'j'\nu} c^{\dagger}_{lj\mu\sigma} c_{l'j'\nu\sigma}, \tag{2}$$

includes also the SO interaction

$$H_{SO}(\theta, \phi) = \xi \sum_{jl} \sum_{\mu\nu} \sum_{\sigma\sigma'} \langle \mu\sigma | \boldsymbol{L} \cdot \boldsymbol{S} | \nu\sigma' \rangle c^{\dagger}_{jl\mu\sigma} c_{jl\nu\sigma'} \tag{3}$$

through which it depends on the magnetization direction (θ, ϕ). Here $\xi = 0.085$ eV is the SO coupling constant for cobalt [9, 11] and $c^{\dagger}$, c are creation and annihilation operators, respectively. The analytical (θ, ϕ) dependence of the SO matrix elements $\langle \mu\sigma | \boldsymbol{L} \cdot \boldsymbol{S} | \nu\sigma' \rangle$ for spins $\sigma, \sigma' = \uparrow, \downarrow$ and all d orbitals μ, ν is given in [21]; similar expressions are used for p orbitals. The Hamiltonian H_0 contains the potentials $V^{\sigma}_{lj\mu} = V^{\sigma}_{l\mu}$ for orbitals μ on every atomic site j in each layer l and the matrices $T^{\sigma}_{lj\mu,l'j'\nu}$ describing electron hopping between neighbouring atoms (the sum over $l'j'$ in equation (2) includes the first and second nearest neighbours of each atom lj) with the aid of the Slater–Koster formalism [22]. The on-site potentials $V^{\sigma}_{l\mu}$ in ferromagnetic Co layers depend on spin σ so that non-zero layer-dependent exchange splittings

$$\Delta^{(l)}_{ex} = V^{\downarrow}_{l\mu} - V^{\uparrow}_{l\mu} \tag{4}$$

are present and they are assumed to be equal for all d orbitals μ in a given layer l.

Two different parametrizations of H_0 are used in the calculations in order to study the effect of sp–d hybridization. The first one, the spd TB model, takes into account all nine s, p and d orbitals while only five d orbitals are used in the other, the d-only TB model. The spd parametrization starts with the TB parameters obtained from the band fit for paramagnetic fcc bulk Co [23]. The paramagnetic two-centre hopping parameters are kept unchanged when used for ferromagnetic bulk and layered Co systems. The on-site potentials $V^{\sigma}_{l\mu}$ are found as follows. First, the on-site potentials for d orbitals in ferromagnetic bulk Co are obtained from the paramagnetic on-site potentials of [23] by introducing bulk exchange splitting $\Delta^{bulk}_{ex} = 1.8$ eV as found in [24]; the bulk s and p on-site potentials retain their corresponding paramagnetic values. Thus, the total occupations n^{bulk}_{s}, n^{bulk}_{p} and n^{bulk}_{d} of s, p and d orbitals, respectively, are determined for bulk ferromagnetic Co. Also, the bulk Co spin magnetic moment is found to be $M_{bulk} = 1.57\,\mu_B$ which is close to values obtained in the *ab initio* calculations [25, 26]. In a Co film, the layer-projected occupation $n^{(l)}_{d}$ of all d orbitals is required to be the same in each AL l and equal to the Co bulk d occupation:

$$n^{(l)}_{d} = n^{bulk}_{d}. \tag{5}$$

Simultaneously, we assume no charge transfer between layers. This, together with equation (5), implies that the sum of layer-projected s and p occupations, $n^{(l)}_{s}$, $n^{(l)}_{p}$, respectively, is also constant throughout the film:

$$n^{(l)}_{s} + n^{(l)}_{p} = n^{bulk}_{s} + n^{bulk}_{p}. \tag{6}$$

These requirements, well satisfied at transition-metal surfaces [26][2], are accompanied by the usual relation

$$\Delta_{\rm ex}^{(l)} = \Delta_{\rm ex}^{\rm bulk} \frac{M_l}{M_{\rm bulk}} \tag{7}$$

giving the local exchange splitting in each Co layer. Then, the on-site potentials $V_{l\mu}^{\sigma}$ for s, p and d orbitals are found by shifting the corresponding bulk values so that the conditions (5) and (7) are fulfilled. The respective potential shifts are layer-dependent. However, in a given layer l, all s and p orbitals are shifted by the same amount; similarly, all d orbitals in layer l have a common shift for given spin. The layer magnetic moments M_l entering equation (7) are obtained self-consistently at the same time. In particular, the moments $M_1 = M_N = 1.80\ \mu_{\rm B}$ at the (001) fcc Co surface, as found for Co(N) films thicker than 7 AL, are enhanced by $0.23\ \mu_{\rm B}$ in comparison with the bulk Co moment; similar enhancement was reported in the *ab initio* calculations [24, 26]. The applied method of determining the spd TB parameters from the conditions (5) and (7) is similar to the approach presented in [27]. It was also used previously in the MA calculations for stepped surfaces in [28].

The second, d-only, TB model, including only d orbitals, is built by adopting the d-orbital hopping parameters and exchange splittings from the full spd model while the on-site potentials are adjusted in such a way that the layer magnetic moments M_l found earlier in the spd model are reproduced exactly. This method is similar to the approach applied previously in the TB models [9–13] based on the canonical TB parameters for d orbitals and the magnetic moments known from *ab initio* calculations.

Apart from the potential shifts discussed above, it is assumed in both presently applied TB models that the on-site potentials $V_{l\mu}^{\sigma}$ in the very surface layers ($l = 1$ and N) include a crystal-field splitting Δ_{cr} between the d orbitals having lobes pointing out of the plane (i.e. $\mu = yz$, zx, $3z^2 - r^2$) and those with lobes lying in the film plane (i.e. $\mu = xy$, $x^2 - y^2$). The value $\Delta_{cr} = 0.22$ eV (cf[3]), close to 5% of the d-band width, is assumed for the Co surface following the previous work [9–13] and the results of the *ab initio* calculations of [29]. Also, recent careful fits [30] to *ab initio* bands of Co monolayers prove the presence of similar crystal-field splittings and imply, for our Co surface, the magnitude of Δ_{cr} close to the assumed value.

The existence of translation symmetry in the film plane implies that the solutions of the Hamiltonian (1) are one-electron Bloch states $|r\boldsymbol{k}\rangle$ labelled with quantum number r and two-dimensional, surface wavevector $\boldsymbol{k}$. These states are spin mixed due to the presence of the SO interaction $H_{\rm SO}(\theta, \phi)$ and their energies $\epsilon_{r\boldsymbol{k}}$ depend on the magnetization direction (θ, ϕ). The total thermodynamic potential of the film is equal to

$$\Omega = \Omega(\theta, \phi) = -k_{\rm B}T \sum_{r\boldsymbol{k}} \ln\left[1 + \exp\frac{\epsilon_{\rm F} - \epsilon_{r\boldsymbol{k}}(\theta, \phi)}{k_{\rm B}T}\right] \tag{8}$$

where $\epsilon_{\rm F}$ is the Fermi energy, T is the temperature and $k_{\rm B}$ is the Boltzmann constant. The MA energy $E_{\rm MA}$ (per surface atom) is then defined in the usual way via the force theorem [14, 31] as the difference

$$E_{\rm MA} = \frac{1}{N_{\rm BZ}}\left[\Omega\left(\theta = 0, \phi = \frac{\pi}{4}\right) - \Omega\left(\theta = \frac{\pi}{2}, \phi = \frac{\pi}{4}\right)\right] \tag{9}$$

of the potential $\Omega(\theta, \phi)/N_{\rm BZ}$ for two different magnetization directions: one perpendicular to the film and another direction lying in the film plane; here $N_{\rm BZ}$ denotes the number of $\boldsymbol{k}$-points

[2] The relation (6) is satisfied also for $l = 1$ when the sp electrons spilled into the vacuum above the Co surface are included into the occupations $n_{\rm s}^{(1)}$, $n_{\rm p}^{(1)}$ in the very surface layer; cf [26]. This assumption is consistent with the TB approach which, normally, does not introduce extra layers of empty spheres in the vacuum region.

[3] For $N = 1$, the value of Δ_{cr} is doubled to $\Delta_{cr} = 0.44$ eV since all lobes of out-of-plane d orbitals point to the vacuum present on the sides of the Co monolayer.

in the BZ. The choice of the in-plane direction along the (010) axis ($\phi = \frac{\pi}{4}$ in equation (9)) is practically irrelevant since the variation of $\Omega(\theta = \frac{\pi}{2}, \phi)$ with the angle ϕ is of the fourth order in the SO coupling constant ξ while E_{MA} is of the order of ξ^2. For the same reason, equation (9) should give a value of E_{MA} very close to the anisotropy constant K_1 obtained within the perturbation theory:

$$E_{\mathrm{MA}} = K_1 + \mathcal{O}(\xi^4). \tag{10}$$

This alternative approach, used in the previous work [9–13], treats the SO interaction H_{SO} as a perturbation and derives K_1 for (001) fcc films from the second-order correction to the thermodynamic potential:

$$\Omega^{(2)} = \frac{1}{2}\sum_{\boldsymbol{k}}\sum_{n\sigma}\sum_{(n'\sigma')\neq(n\sigma)} \frac{f[\epsilon^0_{n'\sigma'}(\boldsymbol{k})] - f[\epsilon^0_{n\sigma}(\boldsymbol{k})]}{\epsilon^0_{n'\sigma'}(\boldsymbol{k}) - \epsilon^0_{n\sigma}(\boldsymbol{k})} |\langle n'\boldsymbol{k}\sigma'|H_{\mathrm{SO}}|n\boldsymbol{k}\sigma\rangle|^2$$
$$= N_{\mathrm{BZ}}(K_0 + K_1\cos^2\theta). \tag{11}$$

Here, $f(\epsilon) = 1/\{1 + \exp[(\epsilon - \epsilon_{\mathrm{F}})/k_{\mathrm{B}}T]\}$ is the Fermi–Dirac occupation factor, $|n\boldsymbol{k}\sigma\rangle$ and $|n'\boldsymbol{k}\sigma'\rangle$ denote the eigenstates of the unperturbed Hamiltonian H_0, equation (2), while $\epsilon^0_{n\sigma}(\boldsymbol{k})$ and $\epsilon^0_{n'\sigma'}(\boldsymbol{k})$ are their corresponding energies; index n (n') numbers bands for each spin σ (σ') at every $\boldsymbol{k}$-point. The explicit expression for the anisotropy constant K_1 in terms of these states and energies is given in [9, 11].

Finite temperature T is used in the present MA calculations because it is convenient from the numerical point of view. For $T > 0$, the sums present in equations (8) and (11) can be done directly and require the use of a relatively small number of $\boldsymbol{k}$-points; on the other hand, integration over BZ poses problems at $T = 0$ in which case special summation techniques, like the triangle method [9] or the state-tracking technique [32], have been developed to achieve convergence of the MA energy. The use of finite T was shown previously [11] not to influence the average value of $E_{\mathrm{MA}} = E_{\mathrm{MA}}(N)$ though the amplitude of MA oscillations is reduced at finite temperature.

3. Results and analysis

3.1. Magnetocrystalline anisotropy with and without sp–d hybridization

The MA energy of (001) fcc Co(N) films has been calculated using the two TB models presented in the previous section. As seen in figure 1, the average value of $E_{\mathrm{MA}} = E_{\mathrm{MA}}(N)$ does not change significantly upon inclusion of s and p orbitals; it is also close to the average value of the MA energy obtained previously within the canonical TB model using only d orbitals [9, 11].

On the other hand, the MA energy calculated in the d-only TB model has oscillations versus the film thickness N remarkably different than $E_{\mathrm{MA}}(N)$ found in the full, spd, TB model. In the latter model, for $N \geqslant 8$ AL, the MA energy $E_{\mathrm{MA}}(N)$ oscillates with period close to 2 AL. Similar oscillations with the same 2 AL period, though with the phase shifted by 1 AL[4]), were also found previously in *ab initio* calculations done by Szunyogh *et al* [16] for multilayer systems including a Co(N) layer. The MA oscillations reported in [16] were obtained for zero temperature which explains why they continue to be present even for very thick films (for $N \gtrsim 40$ in [16]). On the other hand, the oscillations of $E_{\mathrm{MA}}(N)$ shown in figure 1 are calculated for the finite $T = 300$ K and therefore they decay much more quickly (cf [11]; see also the discussion below).

[4] Note that the sign of the presently reported MA energies should be changed to the opposite before comparing with the results shown in figure 1 of [16] since the different sign convention for the MA energy is used there.

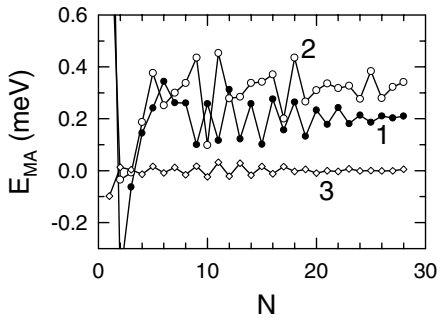

Figure 1. MA energy E_{MA} (cf equation (9)) versus Co film thickness N calculated for (001) fcc Co(N) slabs in the spd (line 1) and d-only (line 2) TB models; $T = 300$ K. The values of E_{MA} for $N = 1$ and 2 in the spd TB model are not visible and they are equal to 1.86 and -0.42 meV, respectively; the value for $N = 1$ in the d-only model is 1.13 meV. Line 3 shows the difference $E_{\mathrm{MA}} - K_1$ found in the spd TB model; K_1 is the MA constant determined within the perturbation theory approach from equation (11).

Figure 1 also presents the difference between E_{MA} found with the force theorem, equation (9), and the anisotropy constant K_1 calculated directly within the perturbation theory via equation (11). As argued earlier in equation (10), E_{MA} and K_1 differ very little: $|E_{\mathrm{MA}} - K_1|$ is not greater than 0.03 meV.

3.2. Analysis of MA oscillations in $\boldsymbol{k}$*- and* N*-spaces*

To understand why sp–d hybridization influences the MA oscillations, one has to answer the basic question of where these oscillations come from. The solution of this problem will be obtained by analysing MA energy in several stages. First, let us note that the MA energy defined by equations (8) and (9) is a sum over the BZ:

$$E_{\mathrm{MA}} = \frac{1}{N_{\mathrm{BZ}}} \sum_{\boldsymbol{k}} e_{\mathrm{MA}}(\boldsymbol{k}). \tag{12}$$

For the sake of simplicity, the MA contributions $e_{\mathrm{MA}}(\boldsymbol{k})$ are symmetrized beforehand so that $e_{\mathrm{MA}}(\boldsymbol{k})$ have the full symmetry of the surface BZ. This can be achieved by taking $e_{\mathrm{MA}}(\boldsymbol{k})$ as half the sum of the MA contributions stemming directly from equations (8) and (9) at $\boldsymbol{k} = (k_x, k_y)$ and $\boldsymbol{k} = (-k_x, k_y)$. Similar BZ symmetrization of MA contributions can be done when E_{MA} is determined via the equations (10) and (11) within the perturbation theory (cf [11]).

The MA contributions $e_{\mathrm{MA}}(\boldsymbol{k})$ come from the whole BZ and the magnitude of $e_{\mathrm{MA}}(\boldsymbol{k}) = e_{\mathrm{MA}}(\boldsymbol{k}, N)$ at a given $\boldsymbol{k}$-point grows with increasing Co film thickness N. Such behaviour, obtained in both TB models applied in this work, was also found earlier for (001) fcc Co slabs within the canonical d-only TB model (see figure 7 in [11]). At present, the dependence of $e_{\mathrm{MA}}(\boldsymbol{k}, N)$ on N is studied more closely at three high-symmetry $\boldsymbol{k}$-points: $\overline{\Gamma}$, $\overline{\mathrm{M}}$, $\overline{\mathrm{X}}$ in figure 2. It is clearly seen that for each of these $\boldsymbol{k}$-points the contribution $e_{\mathrm{MA}}(\boldsymbol{k}, N)$ has roughly a linear dependence on the film thickness N. However, significant oscillations are present on top of the linear function at the $\overline{\Gamma}$- and $\overline{\mathrm{M}}$-points. By generalizing this observation, it is assumed that the relation

$$e_{\mathrm{MA}}(\boldsymbol{k}, N) = e_{\mathrm{MA}}^{\mathrm{con}}(\boldsymbol{k}) + e_{\mathrm{MA}}^{\mathrm{lin}}(\boldsymbol{k})N + e_{\mathrm{MA}}^{\mathrm{osc}}(\boldsymbol{k}, N) \tag{13}$$

holds at any $\boldsymbol{k}$-point. This assumption can be proved rigorously [33] with the use of the Möbius transformation method developed by Umerski [34]. In the present work, the constant

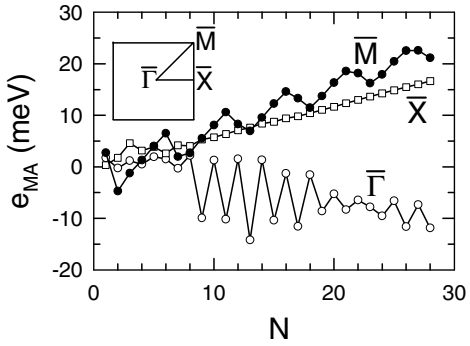

Figure 2. MA contribution $e_{\mathrm{MA}}(\boldsymbol{k})$ versus Co film thickness N calculated in the spd TB model at $\boldsymbol{k} = \overline{\Gamma}, \overline{\mathrm{M}}, \overline{\mathrm{X}}$ for (001) fcc Co(N) slabs; $T = 300$ K. The inset shows the positions of the $\overline{\Gamma}$-, $\overline{\mathrm{M}}$-, $\overline{\mathrm{X}}$-points in the two-dimensional BZ.

term $e^{\mathrm{con}}_{\mathrm{MA}}(\boldsymbol{k})$ and the coefficient $e^{\mathrm{lin}}_{\mathrm{MA}}(\boldsymbol{k})$ of the linear term in equation (13) are found in an approximate manner from values of $e_{\mathrm{MA}}(\boldsymbol{k}, N)$ for $8 \leqslant N \leqslant 28$ by using the least squares method. Then, the oscillatory term $e^{\mathrm{osc}}_{\mathrm{MA}}(\boldsymbol{k}, N)$ is determined for each N from equation (13). This procedure is repeated at every $\boldsymbol{k}$-point.

The obtained term $e^{\mathrm{con}}_{\mathrm{MA}}(\boldsymbol{k})$ and the coefficient $e^{\mathrm{lin}}_{\mathrm{MA}}(\boldsymbol{k})$ are non-zero in the whole BZ. However, when the coefficient $e^{\mathrm{lin}}_{\mathrm{MA}}(\boldsymbol{k})$ is integrated over all the BZ the resultant sum has been found numerically to vanish almost exactly:

$$\frac{1}{N_{\mathrm{BZ}}} \sum_{\boldsymbol{k}} e^{\mathrm{lin}}_{\mathrm{MA}}(\boldsymbol{k}) = 0 + \mathcal{O}(10^{-4}\ \mathrm{meV}). \tag{14}$$

The relation (14) results from the fact that, since $e_{\mathrm{MA}}(\boldsymbol{k})/N \to e^{\mathrm{lin}}_{\mathrm{MA}}(\boldsymbol{k})$ for large N, the quantity $e^{\mathrm{lin}}_{\mathrm{MA}}(\boldsymbol{k})$ is essentially equal to the $\boldsymbol{k}$-resolved MA contribution from an atom in bulk Co metal. Thus, the sum $\sum_{\boldsymbol{k}} e^{\mathrm{lin}}_{\mathrm{MA}}(\boldsymbol{k})$ is the total MA energy (per atom) in bulk Co. However, the MA of a bulk cubic crystal does not contain a second-order term in the SO coupling ξ, i.e. a second-rank anisotropy similar to that found for slabs with reduced symmetry. Indeed, the MA energy of bulk fcc Co starts only with a fourth-rank anisotropy, proportional to ξ^4, so that it is very small when compared to the MA energies of thin films. As a consequence, the total MA energy of (001) Co film can be very well approximated as

$$E_{\mathrm{MA}}(N) = \frac{1}{N_{\mathrm{BZ}}} \sum_{\boldsymbol{k}} e^{\mathrm{con}}_{\mathrm{MA}}(\boldsymbol{k}) + \frac{1}{N_{\mathrm{BZ}}} \sum_{\boldsymbol{k}} e^{\mathrm{osc}}_{\mathrm{MA}}(\boldsymbol{k}, N) = E^{\mathrm{con}}_{\mathrm{MA}} + E^{\mathrm{osc}}_{\mathrm{MA}}(N) \tag{15}$$

which explains qualitatively the dependence of E_{MA} on N seen in figure 1 and also found in the previous MA calculations [7, 9–16, 18, 19]. The average values of the film MA energy is $E^{\mathrm{con}}_{\mathrm{MA}} = 0.20$ meV in the spd TB model and $E^{\mathrm{con}}_{\mathrm{MA}} = 0.32$ meV in the d-only TB model.

The oscillatory MA contribution $e^{\mathrm{osc}}_{\mathrm{MA}}(\boldsymbol{k}, N)$ is found to have significantly larger values only in the vicinity of the $\overline{\Gamma}$- and $\overline{\mathrm{M}}$-points; cf figure 3 for $N = 11$. To visualize this conclusion better, $e^{\mathrm{osc}}_{\mathrm{MA}}(\boldsymbol{k}, N)$ is plotted, in figures 4 and 5, along the diagonal $\overline{\Gamma}$–$\overline{\mathrm{M}}$ of the BZ for several film thicknesses N. As seen in these figures, $e^{\mathrm{osc}}_{\mathrm{MA}}(\boldsymbol{k}, N)$ oscillates with a period close to 2 AL for small $k = |\boldsymbol{k}|$ in both the TB models applied. For $\boldsymbol{k}$ close to the $\overline{\mathrm{M}}$-point (or any of the three other corners of the BZ), $e^{\mathrm{osc}}_{\mathrm{MA}}(\boldsymbol{k}, N)$ has a larger oscillation period: around 5 AL in the spd TB model and around 3.5 AL in the d-only one. The oscillations of $e^{\mathrm{osc}}_{\mathrm{MA}}(\boldsymbol{k}, N)$ at the very $\overline{\Gamma}$- and $\overline{\mathrm{M}}$-points are clearly visible in figure 2.

To quantify how the neighbourhoods of the $\overline{\Gamma}$- and $\overline{\mathrm{M}}$-points contribute to the oscillations of the total MA energy $E_{\mathrm{MA}}(N)$, the oscillatory contribution $e^{\mathrm{osc}}_{\mathrm{MA}}(\boldsymbol{k}, N)$ is integrated over two

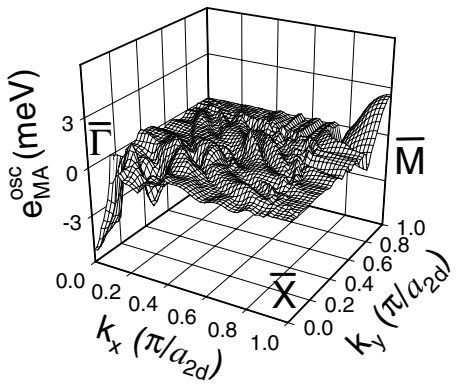

Figure 3. Oscillatory term $e^{\mathrm{osc}}_{\mathrm{MA}}(\boldsymbol{k}, N)$ in the MA contribution $e_{\mathrm{MA}}(\boldsymbol{k}, N)$, equation (13), calculated for (001) fcc Co(11) film ($N = 11$) within the spd TB model; $T = 300$ K. The plot of $e^{\mathrm{osc}}_{\mathrm{MA}}(\boldsymbol{k}, N)$ is shown in a quarter of the BZ and is symmetrical in the other quarters of the BZ.

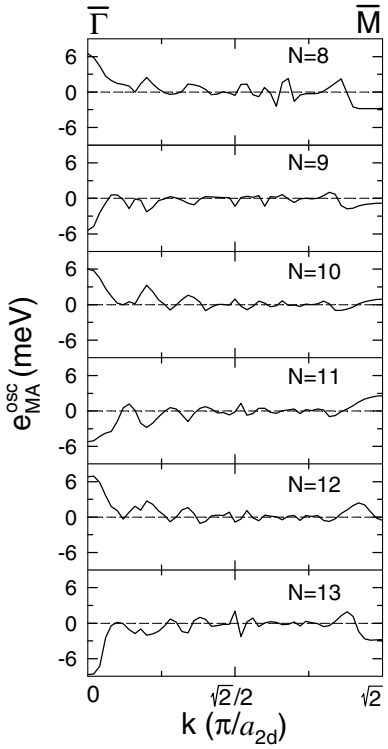

Figure 4. Oscillatory MA term $e^{\mathrm{osc}}_{\mathrm{MA}}(\boldsymbol{k}, N)$ versus $k = \sqrt{k_y^2 + k_y^2}$ along the diagonal $\overline{\Gamma}$–$\overline{\mathrm{M}}$ of the BZ calculated in the spd TB model for (001) fcc Co(N) films ($N = 8$–13); $T = 300$ K.

regions: $\Omega_\Gamma = \{\boldsymbol{k} : |k_i| \leqslant \frac{1}{4}\pi/a_{2\mathrm{d}}, i = x, y\}$, $\Omega_{\mathrm{M}} = \{\boldsymbol{k} : \frac{3}{4}\pi/a_{2\mathrm{d}} \leqslant |k_i| \leqslant \pi/a_{2\mathrm{d}}, i = x, y\}$ which gives two different MA oscillatory terms:

$$E^{\mathrm{osc}}_{\mathrm{MA}}(\Omega_\Gamma, N) = \frac{1}{N_{\mathrm{BZ}}} \sum_{\boldsymbol{k}\in\Omega_\Gamma} e^{\mathrm{osc}}_{\mathrm{MA}}(\boldsymbol{k}, N), \tag{16}$$

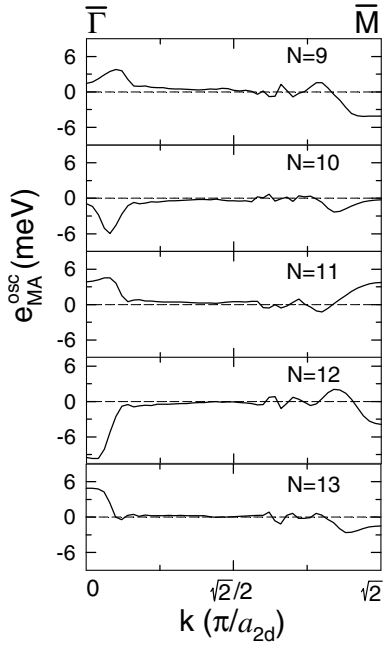

Figure 5. Oscillatory MA term $e^{\rm osc}_{\rm MA}(\boldsymbol{k}, N)$ versus $k = \sqrt{k_y^2 + k_y^2}$ along the diagonal $\overline{\Gamma}$–$\overline{\rm M}$ of the BZ calculated in the d-only TB model for (001) fcc Co(N) films (N = 9–13); T = 300 K.

$$E^{\rm osc}_{\rm MA}(\Omega_{\rm M}, N) = \frac{1}{N_{\rm BZ}} \sum_{\boldsymbol{k}\in\Omega_{\rm M}} e^{\rm osc}_{\rm MA}(\boldsymbol{k}, N). \tag{17}$$

The sum $E^{\rm osc}_{\rm MA}(\Omega_\Gamma, N) + E^{\rm osc}_{\rm MA}(\Omega_{\rm M}, N) + E^{\rm con}_{\rm MA}$ reproduces the total MA energy $E_{\rm MA}$ and its oscillations with good accuracy, especially for $N \geqslant 8$; cf figures 1 and 6. The results shown in figure 6 prove that, in the case of the d-only model, the 2-AL-period oscillations $E^{\rm osc}_{\rm MA}(\Omega_\Gamma, N)$ and the 3.5-AL-period oscillations $E^{\rm osc}_{\rm MA}(\Omega_{\rm M}, N)$ have similar amplitudes so that their superposition $E^{\rm osc}_{\rm MA}(\Omega_\Gamma, N) + E^{\rm osc}_{\rm MA}(\Omega_{\rm M}, N)$, giving effectively $E^{\rm osc}_{\rm MA}(N)$, has a more complex oscillatory dependence with no clear period. On the other hand, in the spd TB model the oscillations $E^{\rm osc}_{\rm MA}(\Omega_{\rm M}, N)$ coming from the corners of the BZ have much smaller amplitude than the term $E^{\rm osc}_{\rm MA}(\Omega_\Gamma, N)$ originating in the centre of the BZ so that the 2-AL-period oscillations $E^{\rm osc}_{\rm MA}(\Omega_\Gamma, N)$ dominate in the sum $E^{\rm osc}_{\rm MA}(\Omega_\Gamma, N)+E^{\rm osc}_{\rm MA}(\Omega_{\rm M}, N) \approx E^{\rm osc}_{\rm MA}(N)$. Thus, an explanation of the qualitatively different MA oscillations patterns found in the spd and d-only TB models is obtained.

3.3. Quantum-well states and MA oscillation periods

To understand better why such a situation takes place and to explain the oscillation periods, it is assumed that the MA oscillations come from QW states with energies close to the Fermi level $\epsilon_{\rm F}$. This assumption, which will be justified *a posteriori*, follows the results of the analysis performed in [13] for (001) fcc Pd(p)/Co(N)/Pd(p) slabs that ended up with the clear conclusion that it is the QW states in the Pd(p) overlayer that are responsible for the oscillations of the MA energy versus the Pd thickness. QW states in the present (001) fcc Co(N) film come from the Bloch states in bulk fcc Co that, in the Co slab, are totally reflected at the boundaries. As a consequence, the z component (i.e. perpendicular to the film surface)

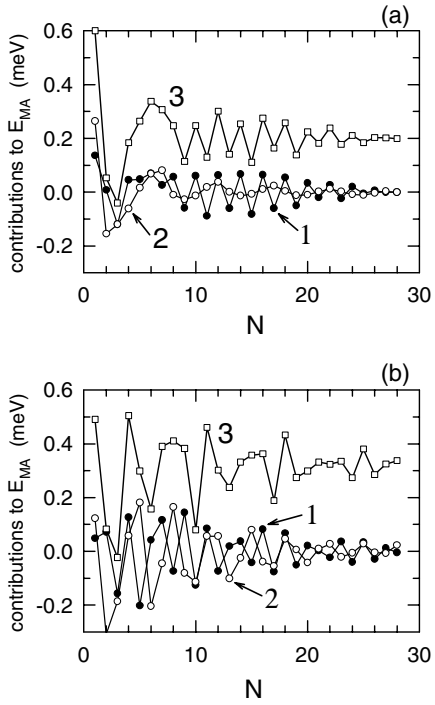

Figure 6. Oscillatory MA contributions $E_{\mathrm{MA}}^{\mathrm{osc}}(\Omega_\Gamma, N)$ (line 1) and $E_{\mathrm{MA}}^{\mathrm{osc}}(\Omega_\mathrm{M}, N)$ (line 2) coming from the BZ regions Ω_Γ and Ω_M, respectively, calculated for (001) fcc Co(N) slabs at $T = 300$ K; cf equations (16) and (17). Line 3 shows the sum $E_{\mathrm{MA}}^{\mathrm{osc}}(\Omega_\Gamma, N) + E_{\mathrm{MA}}^{\mathrm{osc}}(\Omega_\mathrm{M}, N) + E_{\mathrm{MA}}^{\mathrm{con}}$ where the constant MA term $E_{\mathrm{MA}}^{\mathrm{con}}$ is defined in equation (15). (a) spd TB model, (b) d-only TB model.

of the three-dimensional (3D) wavevector $(\boldsymbol{k}, k_z)$ is quantized, which can be described in the phase accumulation picture [35–37] by the general formula

$$k_z = k_z^{(i)} = \frac{\mathrm{i} + \varphi}{N}\frac{2\pi}{a} \tag{18}$$

where $i = 1, \ldots, N$ and φ is a phase shift due to scattering at the boundaries; $\varphi = \varphi_{m\sigma}(\epsilon)$ depends on the bulk band index m, spin σ and also, usually weakly, on the state energy ϵ. The QW state energies $\epsilon_{n\sigma}^0(\boldsymbol{k})$ corresponding to the mth bulk band $\epsilon_{m\sigma}^{\mathrm{b}}(\boldsymbol{k}, k_z)$ can then be approximated by $\epsilon_{m\sigma}^{\mathrm{b}}(\boldsymbol{k}, k_z^{(i)})$. These energies cross the Fermi level ϵ_F periodically when the Co thickness N increases: if the ith QW state crosses ϵ_F for $N = N_i$ the next, $(i + 1)$th, QW state will cross ϵ_F for $N = N_{i+1} = N_i + L$. The corresponding oscillation period is

$$L = \frac{2\pi}{a}[k_{z0}]^{-1} \tag{19}$$

for $k_{z0} \leqslant 0.5\frac{2\pi}{a}$, where k_{z0} is found from the condition

$$\epsilon_{m\sigma}^{\mathrm{b}}(\boldsymbol{k}, k_z = k_{z0}) = \epsilon_\mathrm{F}. \tag{20}$$

For $k_{z0} > 0.5\frac{2\pi}{a}$, we have

$$L = \frac{2\pi}{a}\left[\frac{2\pi}{a} - k_{z0}\right]^{-1} \tag{21}$$

due to the aliasing effect [37]. In this case, the Fermi level ϵ_{F} is successively crossed for $N = \tilde{N}_s$ and $N = \tilde{N}_{s+1} = \tilde{N}_s + L$ by a QW state with $i = \tilde{N}_s - s$ and $i = \tilde{N}_{s+1} - (s+1)$, respectively; here $s = N - i$ relabels $k_z^{(i)}$:

$$k_z = k_z^{(i)} = \left(1 - \frac{s - \varphi}{N}\right)\frac{2\pi}{a}. \tag{22}$$

According to the formula (11), QW states $|n\boldsymbol{k}\sigma\rangle$ corresponding to $k_z^{(i)} \approx k_{z0}$ which cross ϵ_{F} periodically when the film thickness N increases can lead to an oscillatory contribution in the MA energy E_{MA}. The conditions for this to occur are discussed below.

Since the majority-spin d band in bulk and film Co systems is below the Fermi level ϵ_{F}, we first examine only minority-spin bands $\epsilon^{\mathrm{b}}_{m\downarrow}(\boldsymbol{k}, k_z)$ of bulk Co in search of the MA oscillation periods. The minority-spin bands are plotted for fixed $\boldsymbol{k} = \overline{\Gamma}$ and $\overline{\mathrm{M}}$ as a function of k_z in figures 7(a), (b); these two plots actually correspond to the lines Γ–X and X–W–X, respectively, in the 3D BZ. As seen in figure 7(a), for $\boldsymbol{k} = \overline{\Gamma}$, one of the bulk bands $\epsilon^{\mathrm{b}}_{m\downarrow}(\boldsymbol{k}, k_z)$, i.e. the doubly degenerate band Δ_5, crosses ϵ_{F} at $k_z = k_{z0} = 0.528\frac{2\pi}{a}$ in the spd TB model while a similar crossing occurs at $k_{z0} = 0.570\frac{2\pi}{a}$ in the d-only TB model. The two values of k_{z0} correspond to the periods $L = L_\Gamma^{\mathrm{spd}} = 2.12$ AL and $L = L_\Gamma^{\mathrm{d}} = 2.33$ AL, respectively. Both periods are close to 2 AL so that it is legitimate to associate them, and hence also the corresponding QW states, with the calculated MA oscillation contribution $E^{\mathrm{osc}}_{\mathrm{MA}}(\Omega_\Gamma, N)$ coming from the vicinity of the $\overline{\Gamma}$-point. The fact that the obtained oscillation period L differs from 2 AL results in a phase shift seen in the dependence of $E^{\mathrm{osc}}_{\mathrm{MA}}(\Omega_\Gamma, N)$; this shift is especially pronounced in the d-only TB model where the value $L - 2 = L_\Gamma^{\mathrm{d}} - 2 = 0.33$ AL is larger; cf figure 6. In the spd TB model where $L - 2 = L_\Gamma^{\mathrm{spd}} - 2 = 0.12$ AL is small, the dependence $E^{\mathrm{osc}}_{\mathrm{MA}}(\Omega_\Gamma, N)$ has a characteristic beat with a long period of $L_{\mathrm{beat}} = \frac{2}{0.12} \approx 17$ AL due to discrete thickness sampling; cf figure 6. This beat, seen even better in figure 2 where the contribution $e_{\mathrm{MA}}(\boldsymbol{k} = \overline{\Gamma}, N)$ is shown, explains why 2-AL-period oscillations $E^{\mathrm{osc}}_{\mathrm{MA}}(\Omega_\Gamma, N)$ are quenched for $4 \leqslant N \leqslant 7$ in the spd TB model. For $N \leqslant 3$, the notion of QW states becomes highly questionable so that the present analysis is not valid.

For the $\overline{\mathrm{M}}$-point, the bulk bands in the d-only TB model cross the Fermi level at two symmetrical points: $k_z = k_{z0} = 0.301\frac{2\pi}{a}$, $k_z = k_{z0} = 0.699\frac{2\pi}{a}$; cf figure 7. They correspond to the same period of $L = L_{\mathrm{M}}^{\mathrm{d}} = 3.32$ AL according to the formulae (19) and (21). Including the sp–d hybridization results in significant changes of the bulk bands in question, i.e. bands Z_3, so that the positions of the crossing points are modified to $k_{z0} = 0.194\frac{2\pi}{a}$, $0.806\frac{2\pi}{a}$ and the respective period is $L = L_{\mathrm{M}}^{\mathrm{spd}} = 5.15$ AL. Similarly, as for the $\overline{\Gamma}$-point, the exact periods obtained, $L_{\mathrm{M}}^{\mathrm{spd}}$ and $L_{\mathrm{M}}^{\mathrm{d}}$, agree very well with the oscillatory dependence of the MA contribution $E^{\mathrm{osc}}_{\mathrm{MA}}(\Omega_{\mathrm{M}}, N)$ presented in figure 6. This again confirms the link between QW states and the MA oscillations in the (001) fcc Co films.

The values $k_{z0} = 0.528\frac{2\pi}{a}$, $0.194\frac{2\pi}{a}$, $0.806\frac{2\pi}{a}$ found in the spd TB model, and $k_{z0} = 0.570\frac{2\pi}{a}$, $0.301\frac{2\pi}{a}$, $0.699\frac{2\pi}{a}$ obtained in the d-only TB model are extremal radii of the Fermi surface in the (001) direction. This stems from the fact that $\overline{\Gamma}$ and $\overline{\mathrm{M}}$ are stationary points at which the bulk energy bands have extrema as functions of $\boldsymbol{k}$. Each of the listed values of k_{z0} is modified when $\boldsymbol{k}$ moves away from the respective high-symmetry $\boldsymbol{k}$-point, $\overline{\Gamma}$ or $\overline{\mathrm{M}}$. However, the changes of $k_{z0} = k_{z0}(\boldsymbol{k})$ are relatively small in some neighbourhood of the high-symmetry point so that the MA contributions coming from such a region have similar oscillation periods $L = L[k_{z0}(\boldsymbol{k})]$ and thus they add up to a sizeable MA term oscillating with a clear period. The area of the contributing region and, as a consequence, the oscillation amplitude are inversely proportional to the curvature of the respective bulk band as a function of $\boldsymbol{k}$, similar to that found in the case of oscillations of exchange coupling; cf [39–42]; see also discussion below.

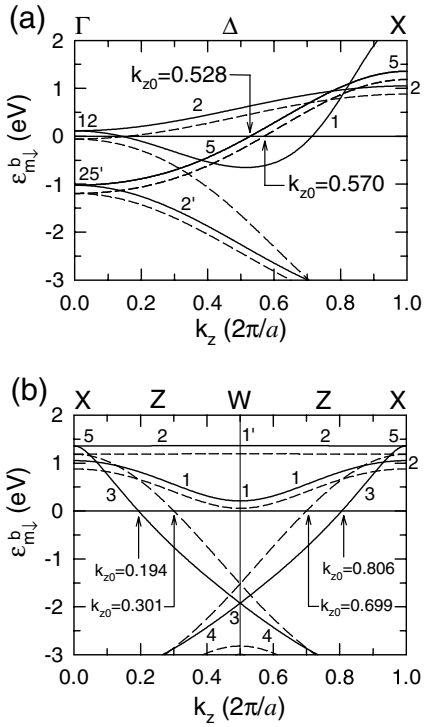

Figure 7. Minority-spin energies $\epsilon^{\mathrm{b}}_{m\downarrow}(\boldsymbol{k}, k_z)$ in bulk fcc Co versus z component of the 3D wavevector $(\boldsymbol{k}, k_z)$. The energies are calculated for fixed (a) $\boldsymbol{k} = \overline{\Gamma}$ and (b) $\boldsymbol{k} = \overline{\mathrm{M}}$ in the spd (full curves) and d-only (broken curves) TB models without SO coupling. The state symmetries are marked with the standard symbols (see, e.g., [38]). The horizontal line denotes the Fermi energy $\epsilon_{\mathrm{F}} = 0$.

There are also other extremal radii of the Fermi surface than those listed above. The extra radii k_{z0} are found for minority spin at $\boldsymbol{k} = \overline{\Gamma}$ (see figure 7(a)), but also for majority spin at the well-known 'belly' and 'neck' stationary points, i.e. at $\boldsymbol{k} = \overline{\Gamma}$ and $\boldsymbol{k} = (\pm 0.74\frac{\pi}{a_{2\mathrm{d}}}, 0)$ (and $\boldsymbol{k} = (0, \pm 0.74\frac{\pi}{a_{2\mathrm{d}}})$), for Co, respectively. However, all these additional extremal radii, i.e. all those not marked in figure 7, give apparently weak contributions to MA as no extra oscillations, with periods other than 2 AL, are seen in $E^{\mathrm{osc}}_{\mathrm{MA}}(\Omega_\Gamma, N)$ (cf figure 6). We also find that the $\boldsymbol{k}$-resolved MA contribution $e_{\mathrm{MA}}(\boldsymbol{k})$ does not oscillate in the vicinity of the 'neck' points; see figure 3. The reason for this is rapid variation of the additional $k_{z0}(\boldsymbol{k})$ around the corresponding stationary points due to large curvatures of the involved sp bands or, in the case of $k_{z0} = 0.14\frac{\pi}{a_{2\mathrm{d}}}$ seen in figure 7(a), due to a very small distance of the d bands 1, 2 from the Fermi level ϵ_{F} for small k_z.

The mechanism of how QW states induce the investigated MA oscillations is visualized in figures 8 and 9 which show the minority-spin energy bands around the $\overline{\Gamma}$- and $\overline{\mathrm{M}}$-points for a few selected film thicknesses. To pick up, from all the energy bands, the energies of the QW states involved in the MA oscillations coming from a given k_{z0}, we calculate the quantity

$$g^{\downarrow}_n(\boldsymbol{k}, k_z) = \frac{2}{N}\sum_{\mu}\left|\sum_{l=1}^{N}\exp(\mathrm{i}k_z z_l)a^{\downarrow}_{nl\mu}(\boldsymbol{k})\right|^2 \tag{23}$$

for each minority-spin state

$$|n\boldsymbol{k}\downarrow\rangle = \sum_{l\mu} a^{\downarrow}_{nl\mu}(\boldsymbol{k})|\boldsymbol{k}l\mu\downarrow\rangle \tag{24}$$

and demand that

$$g^{\downarrow}_{n}(\boldsymbol{k}, k_z) \geqslant w \tag{25}$$

for some $k_z \in [k_{z0} - \Delta k_z, k_{z0} + \Delta k_z]$. Here, $z_l = la/2$ is the z coordinate of the lth atomic plane and each basis state $|\boldsymbol{k}l\mu\downarrow\rangle$ is a two-dimensional Bloch state formed from atomic orbitals μ on all sites j in AL l; cf [9, 11, 13]. Since the eigenstates $|n\boldsymbol{k}\downarrow\rangle$ are either z-odd or z-even as far as the mirror symmetry with respect to the middle film plane $z = z_{\mathrm{mid}}$ is concerned, the space variation of a QW state $|n\boldsymbol{k}\downarrow\rangle$ derived from a bulk state

$$|m\boldsymbol{k}k_z^{(i)}\downarrow\rangle = \sum_{\mu} b^{\downarrow}_{m\mu}(\boldsymbol{k}, k_z^{(i)})|\boldsymbol{k}k_z^{(i)}\mu\downarrow\rangle \tag{26}$$

(here $|\boldsymbol{k}k_z^{(i)}\mu\downarrow\rangle$ are 3D basis Bloch states) is given approximately by either

$$a^{\downarrow}_{nl\mu}(\boldsymbol{k}) = \sqrt{\frac{2}{N}} b^{\downarrow}_{m\mu}(\boldsymbol{k}, k_z^{(i)}) \cos k_z^{(i)}(z_l - z_{\mathrm{mid}}) \tag{27}$$

or

$$a^{\downarrow}_{nl\mu}(\boldsymbol{k}) = \sqrt{\frac{2}{N}} b^{\downarrow}_{m\mu}(\boldsymbol{k}, k_z^{(i)}) \sin k_z^{(i)}(z_l - z_{\mathrm{mid}}) \tag{28}$$

depending on the parities (z-even or z-odd) of the state $|n\boldsymbol{k}\downarrow\rangle$ and orbital μ. The relations (27) and (28) hold well in the interior of the film while they become modified near the surfaces. Thus, for a thick film, the quantity $g^{\downarrow}_{n}(\boldsymbol{k}, k_z)$ calculated for such a QW state $|n\boldsymbol{k}\downarrow\rangle$ is close to 1 when $k_z \approx k_z^{(i)}$; it is somewhat smaller for thinner films. On the other hand, $g^{\downarrow}_{n}(\boldsymbol{k}, k_z)$ is close to 0 when k_z differs significantly from $k_z^{(i)}$. Thus, the condition (25) selects the QW states with $k_z^{(i)} \approx k_{z0}$. The threshold value is taken to be $w = 0.5$ for the vicinity of the $\overline{\Gamma}$-point, shown in figure 8, since deviations from the relations (27) and (28) for QW states $|n\boldsymbol{k}\downarrow\rangle$ with a short period close to 2 AL lead easily to a significant decrease of $g^{\downarrow}_{n}(\boldsymbol{k}, k_z)$. A larger, more selective, value of $w = 0.7$ can be used around the $\overline{\mathrm{M}}$-point where the interesting QW states have longer periods. Checking the condition (25) for k_z from the interval $[k_{z0} - \Delta k_z, k_{z0} + \Delta k_z]$, instead of at one point $k_z = k_{z0}$ only, allows for identification of QW states from a larger neighbourhood of the Fermi level ϵ_{F}; for this purpose the value $\Delta k_z = 0.05\frac{2\pi}{a}$ is chosen.

As seen in figure 8, the QW states around the $\overline{\Gamma}$-point identified by using the condition (25) with $k_{z0} = 0.528\frac{2\pi}{a}$ (corresponding to $L = 2.12$ AL), in the spd TB model, come in pairs which are degenerate at $\boldsymbol{k} = \overline{\Gamma}$, similar to the bulk band Δ_5 in figure 7 from which these QW states originate. This resembles the situation found previously [12, 13] for Pd(p)/Co(N)/Pd(p) systems where similar pairs of QW states present in the Pd overlayer near the top of the d-band were proved to cause MA oscillations versus the Pd thickness p. In fact, it is the same branch of the bulk d-band, i.e. band Δ_5, though in different energy regimes that is involved in both cases. According to the formula (11), two states $|n\boldsymbol{k}\downarrow\rangle$, $|n'\boldsymbol{k}\downarrow\rangle$ forming one of the described pairs contribute significantly to MA when their energies are close to each other and they lie on two sides of the Fermi level ϵ_{F} or within a few kT from it; cf [13]. This situation takes place when the pair energies are close to ϵ_{F} at $\boldsymbol{k} = \overline{\Gamma}$ where they are degenerate. In the spd TB model, such favorable alignment of the QW state pairs is found, in particular, for $N = 11$, but not for $N = 12$, as seen in figure 8, and also for other odd film thicknesses N in the range $8 \leqslant N \leqslant 24$, but not for even values of N. Thus, we obtain a correlation between the positions of the QW state pairs and the dependence on N of the MA contribution $E^{\mathrm{osc}}_{\mathrm{MA}}(\Omega_\Gamma, N)$

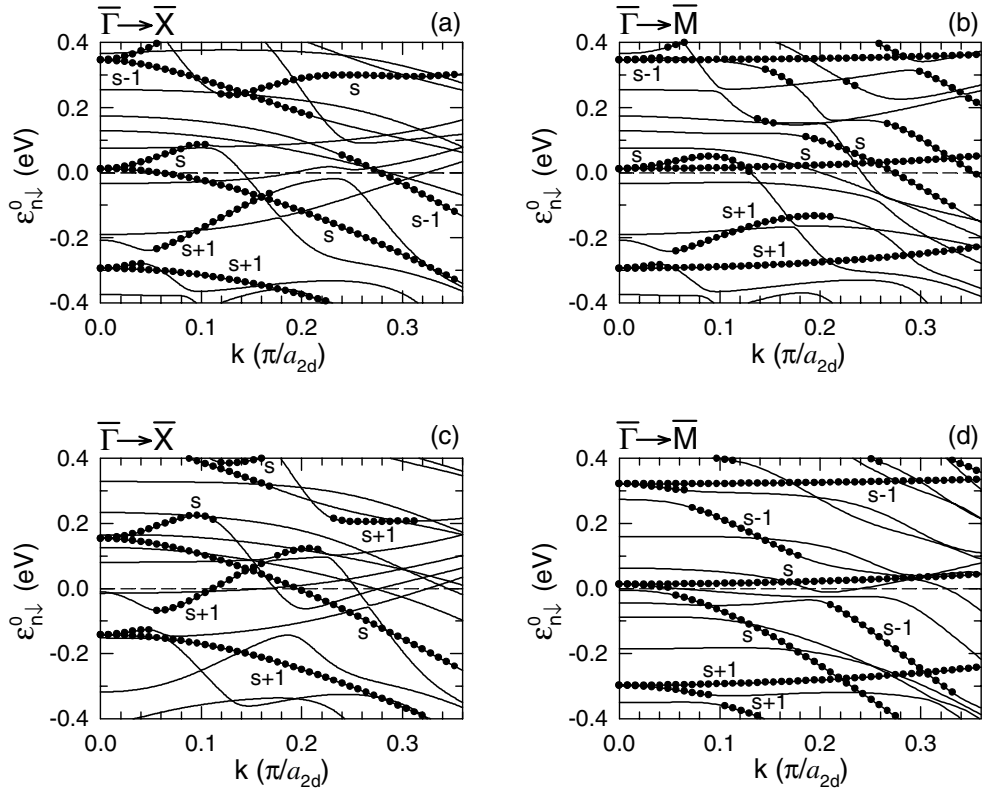

Figure 8. Minority-spin energies $\epsilon^0_{n\downarrow}(\boldsymbol{k})$ in the (001) fcc Co(N) film plotted in the vicinity of the $\overline{\Gamma}$-point versus $k = \sqrt{k_x^2 + k_y^2}$ along the lines $\overline{\Gamma}$–$\overline{\mathrm{X}}$ (plots (a), (c)) and $\overline{\Gamma}$–$\overline{\mathrm{M}}$ (plots (b), (d)). The energies are calculated for $N = 11$ (plots (a), (b)), $N = 12$ (plot (c)) in the spd TB model, and for $N = 12$ in the d-only TB model (plot (d)), without SO coupling. The bulletted lines (•) denote energies of those states $|n\boldsymbol{k}\downarrow\rangle$ for which there exists $k_z \in [0.528\frac{2\pi}{a} - \Delta k_z, 0.528\frac{2\pi}{a} + \Delta k_z]$ in the spd model, or $k_z \in [0.57\frac{2\pi}{a} - \Delta k_z, 0.57\frac{2\pi}{a} + \Delta k_z]$ in the d-only model, such that $g^{\downarrow}_n(\boldsymbol{k}, k_z)$, equation (23), is larger than $w = 0.5$; $\Delta k_z = 0.05\frac{2\pi}{a}$. These QW states are marked with indices $s, s \pm 1$ where $s = N - i$ relabels $k_z^{(i)}$, cf equation (22); the value of s is the same in plots (a)–(c) but can be different in plot (d). The horizontal broken line denotes $\epsilon_{\mathrm{F}} = 0$.

oscillating with the period close to 2 AL; cf figure 6. This scenario is supported by the fact that states $|n\boldsymbol{k}\downarrow\rangle$, $|n'\boldsymbol{k}\downarrow\rangle$ belonging to different pairs derived from band Δ_5 give a very small contribution to MA, even if their energies are favourably placed. This happens because the formula (11) contains expressions like

$$\sum_{l=1}^{N} [a^{\downarrow}_{nl\mu}]^* a^{\downarrow}_{n'l\nu} \tag{29}$$

(cf [12, 13]) which are close to 0 when the two QW states $|n\boldsymbol{k}\downarrow\rangle$, $|n'\boldsymbol{k}\downarrow\rangle$ are both given by equations (27) and (28) and the corresponding values of $k_z^{(i)}$ and $k_z^{(i')}$ are different (i.e. $i \neq i'$ while the respective phase shifts φ, φ' are very similar). It can also be checked numerically that the MA contribution coming solely from the pair states present in the vicinity of the Fermi level ϵ_{F}, namely closer than 0.4 eV from ϵ_{F}, accounts for around 90% of the 2-AL-period MA oscillations $E^{\mathrm{osc}}_{\mathrm{MA}}(\Omega_\Gamma, N)$.

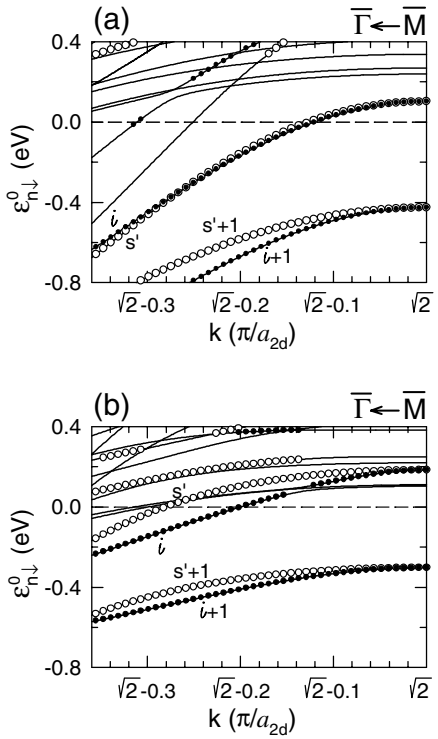

Figure 9. Minority-spin energies $\epsilon^0_{n\downarrow}(\boldsymbol{k})$ in the (001) fcc Co(N) film in the vicinity of the $\overline{\mathrm{M}}$-point plotted versus $k = \sqrt{k_y^2 + k_y^2}$ along the diagonal $\overline{\Gamma}$–$\overline{\mathrm{M}}$ of the BZ. The energies are calculated for $N = 13$ in the (a) spd TB and (b) d-only TB models, without SO coupling. The bulletted lines (•) denote energies of those states $|n\boldsymbol{k}\downarrow\rangle$ for which $g^{\downarrow}_n(\boldsymbol{k}, k_z)$, equation (23), is larger than $w = 0.7$ for some $k_z \in [0.194\frac{2\pi}{a} - \Delta k_z, 0.194\frac{2\pi}{a} + \Delta k_z]$ in plot (a), and for some $k_z \in [0.301\frac{2\pi}{a} - \Delta k_z, 0.301\frac{2\pi}{a} + \Delta k_z]$ in plot (b); $\Delta k_z = 0.05\frac{2\pi}{a}$. These QW states are also marked with indices i, $i + 1$ where i labels $k_z^{(i)}$, equation (18). Similarly, the lines with open circles (∘) correspond to QW states with $k_z \in [0.806\frac{2\pi}{a} - \Delta k_z, 0.806\frac{2\pi}{a} + \Delta k_z]$ in plot (a) and $k_z \in [0.699\frac{2\pi}{a} - \Delta k_z, 0.699\frac{2\pi}{a} + \Delta k_z]$ in plot (b), and they are marked with the respective indices $s' = N - i', s' + 1$; cf equation (22). The values of i and s' in plot (b) are different, in general, from those in plot (a). The horizontal broken line denotes $\epsilon_{\mathrm{F}} = 0$.

In the case of the oscillations $E^{\mathrm{osc}}_{\mathrm{MA}}(\Omega_{\mathrm{M}}, N)$ arising in the neighbourhood of the $\overline{\mathrm{M}}$-point, one of the QW states $|n\boldsymbol{k}\downarrow\rangle$, $|n'\boldsymbol{k}\downarrow\rangle$ contributing in the formula (11) comes from the minority-spin non-degenerate bulk band Z_3 and corresponds to $k_z^{(i)}$ close to one of the determined extremal radii, i.e. $k_{z0} = 0.194\frac{2\pi}{a}$ or $0.806\frac{2\pi}{a}$ in the spd TB model, while the second state can originate from other bulk bands and its energy is not limited to the immediate vicinity of ϵ_{F}. It should be noted here that an eventual contribution from the QW states $|n\boldsymbol{k}\downarrow\rangle$ with $k_z^{(i)} \approx 0.194\frac{2\pi}{a}$ coupled to the QW states $|n'\boldsymbol{k}\downarrow\rangle$ corresponding to $k_z^{(i')} \approx 0.806\frac{2\pi}{a}$ is not significant despite the energies of such states, both originating from bulk band Z_3, being very close to each other near ϵ_{F}; cf figure 9; a similar conclusion is also valid in the d-only TB model. This happens because the formula (11) for E_{MA} is built of expressions similar to (29) (cf [9, 11, 13]) which become small when $k_z^{(i)}$ and $k_z^{(i')}$ lie far from each other.

By comparing figures 4 and 5 with 8, 9, one notes that the shape of the $\boldsymbol{k}$-resolved MA oscillatory contribution $e^{\mathrm{osc}}_{\mathrm{MA}}(\boldsymbol{k}, N)$ near the $\overline{\Gamma}$- and $\overline{\mathrm{M}}$-points is correlated with the position of

the QW bands corresponding to the respective extremal radii. In particular, the effective region contributing to MA oscillations around the $\overline{\mathrm{M}}$-point is determined roughly by the maximal value κ_{m} of the nearest distance, from the $\overline{\mathrm{M}}$-point, at which the QW bands lying above the Fermi level ϵ_{F} cross ϵ_{F}; see figure 9. The area of this region grows as κ_{m}^2, which explains why, as mentioned above, it is inversely proportional to the curvature of the QW bands (or the bulk band they originate from) which are described by a quadratic function of $\boldsymbol{k}$ near the $\overline{\mathrm{M}}$-point. This argument elucidates why the oscillatory contribution $E_{\mathrm{MA}}^{\mathrm{osc}}(\Omega_{\mathrm{M}}, N)$ coming from the neighbourhood of the $\overline{\mathrm{M}}$-point is a few times smaller in the spd TB model than in the d-only model (cf figure 6) which, as shown before, implies different behaviour of the total MA energy $E_{\mathrm{MA}}(N)$ in the two TB models. Indeed, as seen in figure 9, the interesting QW bands are much more bent downwards near the $\overline{\mathrm{M}}$-point when the spd hybridization is present.

Having established the origin of the MA oscillations, one can easily explain why they decay with increasing Co film thickness N; see figures 1 and 6. Indeed, when the film becomes thicker the energies of the QW state pairs existing near the $\overline{\Gamma}$-point become closer to each other so that more than one pair can contribute to the MA for a given thickness N. Consequently, the amplitude of the MA oscillations, arising as the QW energies pass through the Fermi level ϵ_{F} with changing N becomes smaller. Introduction of a finite temperature works in a similar way by smoothing the step of the Fermi–Dirac function $f(\epsilon)$.

While MA oscillation periods are determined by the extremal radii of bulk Fermi surface, the phases of the MA oscillations depend on the precise positions of the energies of the corresponding QW states with respect to the Fermi level ϵ_{F} as already noted above when figures 6 and 8 were compared. These positions depend, in particular, on the phase shift φ present in the quantization formula (18) which defines values of $k_z^{(i)}$. Since φ is modified when the Co surfaces of Co(N) film are replaced with Co/Cu, or similar, interfaces, as assumed in [16], the phase of the 2-AL-period MA oscillations can change appropriately, which can explain the 1-AL phase shift between the present MA results and the ones reported in [16]. Another reason for this effect could be a small difference between bulk magnetic moments found in the two calculations in question which results in slightly different positions of the Fermi levels ϵ_{F}.

4. Concluding remarks

The reported calculations show that the TB approach yields the MA energy of a (001) fcc Co(N) film that oscillates versus the film thickness N with a clear period, close to 2 AL, *once* the sp–d hybridization is included. This result agrees very well with the oscillatory N dependence of the MA energy found by Szunyogh *et al* [16] for Co/Cu systems including a Co(N) layer. In the present paper it is proved that the 2-AL-period MA oscillations come from the pairs of minority-spin QW states occurring near the Fermi level around the $\overline{\Gamma}$-point in the surface BZ. It is also shown that there is a second MA oscillatory contribution, with a larger period, coming from QW states in the neighbourhood of the $\overline{\mathrm{M}}$-point, but this contribution is dominated by the 2-AL-period MA term when the sp–d hybridization is present. The exact periods of these two MA oscillatory contributions are determined by the extremal radii, in the (001) direction, of the minority-spin bulk Fermi surface at the $\overline{\Gamma}$- and $\overline{\mathrm{M}}$-points. Thus, high-symmetry $\boldsymbol{k}$-points are shown to play an important role in the phenomenon of MA oscillations.

The extremal radius $k_{z0} = 0.528\frac{2\pi}{a}$ found at the $\overline{\Gamma}$-point, in the spd TB model, gives the dominant period of 2.12 AL and it matches very well the position $q_0 = 0.5$ (leading to the MA period of $q_0^{-1} = 2$ AL) of the main maximum of the discrete Fourier transform $F(q)$ obtained in [16] from the MA energy as a function of the Co layer thickness N. The two other

extremal radii $k_{z0} = 0.194\frac{2\pi}{a}$ and $0.806\frac{2\pi}{a}$, which correspond to the $\overline{\mathrm{M}}$-point MA contribution with period of 5.15 AL, coincide almost exactly with the positions $q = 0.2$ and 0.8 of the side maxima where $F(q)$ is around four times smaller than at the main maximum $q_0 = 0.5$. This proves that these additional maxima, though they were not discussed in [16], are not artefacts but represent an extra small oscillatory MA term. Thus, it can be concluded that the TB approach including spd hybridization can predict MA oscillation patterns with an accuracy close to that of *ab initio* calculations. This stems from the fact that the oscillation periods are determined on the basis of the bulk Fermi surface found by using TB parameters which were obtained in [23] by fitting *ab initio* bulk bands. An advantage of using the parametrical TB model is that, due to its high numerical efficiency, one can diagonalize the full film Hamiltonian and, consequently, through appropriate analysis of MA energy, one can identify individual quantum states responsible for the MA oscillations. This goal is hard to achieve within the *ab initio* approach since successful *ab initio* calculations of MA energies for sufficiently thick films are based on a Green function formalism, like the screened Korringa–Kohn–Rostoker (KKR) method used in [14–16].

The present TB calculations also show that the MA energies found with the aid of the force theorem (used, e.g., in [7, 8, 14–16, 19]) coincide almost exactly with the results obtained within the second-order perturbation theory TB approach developed in this author's previous work on MA [9–13]. This conclusion implies that an eventual MA contribution due to degeneracies of quantum states at the Fermi level, discussed in [18], is negligible for (001) fcc Co films.

Experimentally, the oscillations of the MA energy with the thickness of the (001) fcc Co layer have been reported only by Krams *et al* [4] who found the onset of 2 AL MA oscillations decaying very quickly with N. As already mentioned, the lack of MA oscillations in most experiments can be attributed to the surface quality. Indeed, one can expect that the investigated MA oscillations in Co films are greatly diminished when their period of 2 AL is shorter than the vertical amplitude of the surface roughness profile. Another reason can be due to the fact that the responsible QW states correspond to small in-plane wavevectors $\boldsymbol{k}$, which implies that the surface has to be flat over relatively large areas if these QW states are to propagate well.

Acknowledgments

This work was supported by the research project no 2P03B 032 22 financed by the State Committee for Scientific Research (Poland) in the years 2002–2004. I would also like to gratefully acknowledge the support of the Engineering and Physical Sciences Research Council (UK) during my visits to Imperial College in 2001.

References

[1] Chapert C, Le Dang K, Beauvillain P, Hurdequint H and Renard D 1986 *Phys. Rev.* B **34** 3192
[2] Johnson M T, de Vries J J, McGee N W E, aan de Stegge J and den Broeder F J A 1992 *Phys. Rev. Lett.* **69** 3575
[3] Lee J, Lauhoff G and Bland J A C 1997 *Phys. Rev.* B **56** R5728
[4] Krams P, Lauks F, Stamps R L, Hillebrands B and Güntherodt G 1992 *Phys. Rev. Lett.* **69** 3674
[5] Weber W, Bischof A, Allenspach R, Würsch Ch, Back C H and Pescia D 1996 *Phys. Rev. Lett.* **76** 342
[6] Bounough A, Train C, Beauvillain P, Bruno P, Chappert C, Megy R and Veillet P 1997 *J. Magn. Magn. Mater.* **165** 484
[7] Gay J G and Richter R 1987 *J. Appl. Phys.* **61** 3362
[8] Kyuno K, Yamamoto R and Asano S 1993 *J. Magn. Magn. Mater.* **126** 268
[9] Cinal M, Edwards D M and Mathon J 1994 *Phys. Rev.* B **50** 3754
[10] Cinal M, Edwards D M and Mathon J 1995 *J. Magn. Magn. Mater.* **140–144** 681
[11] Cinal M and Edwards D M 1997 *Phys. Rev.* B **55** 3636
[12] Cinal M and Edwards D M 1998 *Phys. Rev.* B **57** 100

[13] Cinal M 2001 *J. Phys.: Condens. Matter* **13** 901
[14] Szunyogh L, Újfalussy B and Weinberger P 1995 *Phys. Rev.* B **51** 9552
[15] Újfalussy B, Szunyogh L and Weinberger P 1996 *Phys. Rev.* B **54** 9883
[16] Szunyogh L, Újfalussy B, Blaas C, Pustugova U, Sommers C and Weinberger P 1997 *Phys. Rev.* B **56** 14036
[17] Lorenz R and Hafner J 1996 *Phys. Rev.* B **54** 15937
[18] Lessard A, Moos T H and Hübner W 1997 *Phys. Rev.* B **56** 2594
[19] Guo G Y 1999 *J. Phys.: Condens. Matter* **11** 4329
[20] Cinal M and Umerski A 2002 in preparation
[21] Abate E and Asdente M 1965 *Phys. Rev.* **140** A1303
[22] Slater J C and Koster G F 1954 *Phys. Rev.* **94** 1498
[23] Papaconstantopoulos D A 1986 *Handbook of the Band Structure of Elemental Solids* (New York: Plenum)
[24] Li C and Freeman A J 1988 *J. Magn. Magn. Mater.* **75** 53
[25] Min B I, Oguchi T and Freeman A J 1986 *Phys. Rev.* B **33** 7852
[26] Aldén M, Mirbt S, Skriver H L, Rosengaard N M and Johansson B 1992 *Phys. Rev.* B **46** 6303
[27] Tersoff J and Falicov L M 1982 *Phys. Rev.* B **26** 6186
[28] Cinal M, Umerski A, Edwards D M and Inoue J 2001 *Surf. Sci.* **493** 744–7
[29] Galagher J M and Haydock R 1978 *Phil. Mag.* B **38** 155
[30] Cinal M, Umerski A and Edwards D M in preparation
[31] Daalderop G H O, Kelly P J and Schuurmans M F H 1990 *Phys. Rev.* B **41** 11919
[32] Wang D-S, Wu R and Freeman A J 1993 *Phys. Rev. Lett.* **70** 869
Wang D-S, Wu R and Freeman A J 1993 *Phys. Rev.* B **47** 14932
[33] Umerski A 2002 in preparation
[34] Umerski A 1997 *Phys. Rev.* B **55** 5266
[35] Echenique P M and Pendry J B 1978 *J. Phys. C: Solid State Phys.* **11** 2065
[36] Smith N V, Brookes N B, Chang Y and Johnson P D 1994 *Phys. Rev.* B **49** 332
[37] Niklasson A M N, Mirbt S, Skiver H L and Johansson B 1997 *Phys. Rev.* B **56** 3276
[38] Mueller F M, Freeman A J, Dimmock J O and Furdyna A M 1970 *Phys. Rev.* B **1** 4617
[39] Edwards D M, Mathon J, Muniz R B and Phan M S 1991 *Phys. Rev. Lett.* **67** 493
[40] Mathon J, Villeret M and Edwards D M 1992 *J. Phys.: Condens. Matter* **4** 9873
[41] Mathon J, Villeret M, Muniz R B, d'Albuquerque e Castro J and Edwards D M 1995 *Phys. Rev. Lett.* **74** 3696
[42] Mathon J, Villeret M, Umerski A, Muniz R B, d'Albuquerque e Castro J and Edwards D M 1997 *Phys. Rev.* B **56** 11797